MgII radius-luminosity relation: applications to the BLR structure and cosmology

Michal Zajaček

B. Czerny, N. Khadka, M. L. Martínez-Aldama, S. Panda, R. Prince, B. Ratra, M. Naddaf

Faculty of Science, Masaryk University

The Restless Nature of AGN ⋆ 10 years later

June 27, 2023 - Napoli

Reverberation mapping of galactic nuclei

Different wavelengths probe different scales of an accretion flow

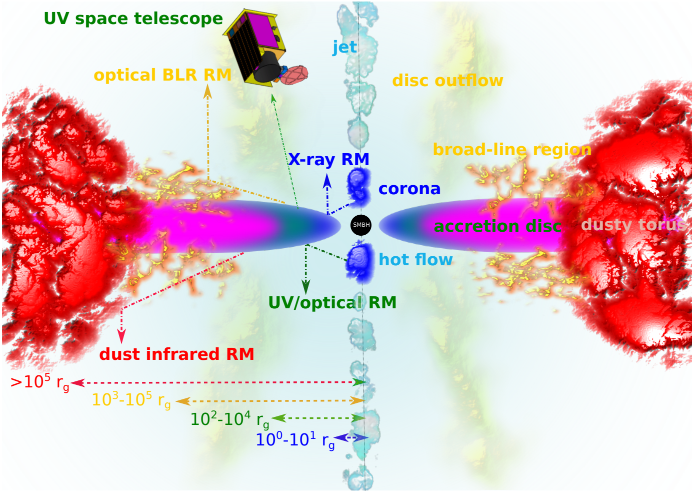

Reverberation mapping of galactic nuclei – results

- **mean radius of the BLR**: $R_{\rm BLR} \sim c\tau_{\rm rest}$
- the **virial mass of the SMBH**: $M_{\rm vir} = \frac{f_{\rm vir} c\tau_{\rm rest} \mathrm{FWHM}^2}{G}$
- **radius-luminosity relation:** $R_{\rm BLR} = CL_{\rm mon}^{\gamma} \rightarrow \tau = \beta + \gamma \log L_{\rm mon}$

The power-law slope is expected to be close to 0.5.
This follows from simple photoionization theory of a BLR cloud:

$$U = \frac{Q_{\rm ion}(H)}{4\pi R^2 c n_{\rm e}}\,, Q_{\rm ion}(H) = \int_{\nu_i}^{+\propto} \frac{L_\nu}{h\nu}{\rm d}\nu$$

Under the assumption $Un_{\rm e}$ $\sim$konst. for different sources, we can derive $R \propto L^{1/2}$

Hβ Radius-luminosity relation

- Hβ broad line was mostly used to obtain time delays for lower-redshift sources ($0.0023 \leq z \leq 0.89$).
- Earlier data had a small scatter (lower accreting, variable sources), later the scatter increased due to the presence of higher-accreting sources.

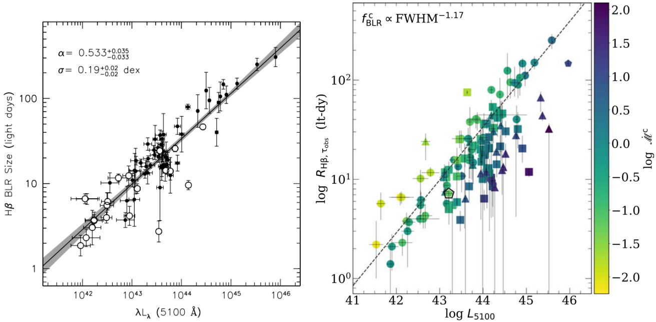

Bentz+13 (71 sources) and Martinez-Aldama+2019 (117 sources)

MgII Radius-luminosity relation

- Czerny+2019, Zajaček+2020, and Zajaček+2021 construct first robust MgII radius-luminosity relations using higher-redshift, luminous sources in the range $0.0033 \leq z \leq 1.89$.
- 10 sources (2xNGC 4151, 6 SDSS-RM, CT252 and CTS C30.10: $\tau = 562^{+116}_{-68}$ days)

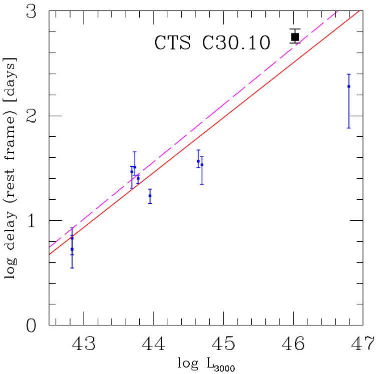

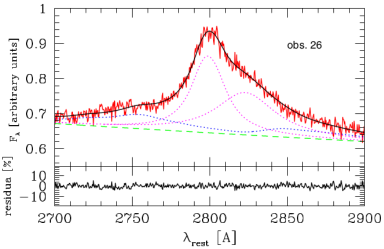

MgII Radius-luminosity relation

- Zajaček+2020 add one more measurement (HE 0413, $z = 1.37648$, $\tau = 302.6^{+28.7}_{-33.1}$ days) and show that the departure is correlated with the accretion rate
- Correlation: $\dot{\mathcal{M}} = 26.2(L_{44}/\cos\theta)^{3/2} m_7^{-2}$, $\Delta\tau = \log\left(\tau_{\rm obs}/\tau_{RL}\right)$

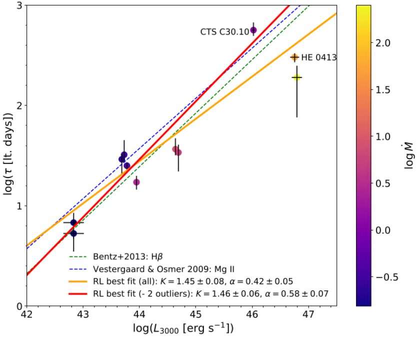

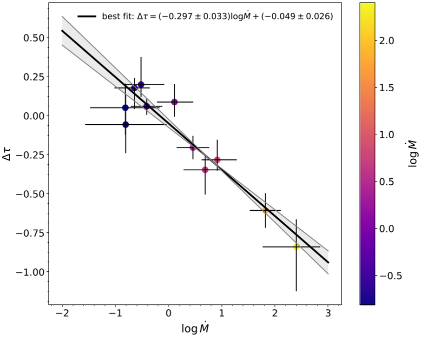

MgII Radius-luminosity relation

- In Zajaček+2021, we perform reverberation mapping of the quasar HE 0435 ($z = 1.2231$, $\tau = 296^{+13}_{-14}$ days)
- 57+6 SDSS-RM (Homayouni+20, Shen+16), 2xNGC4151 (Metzroth+06), CT 252 (Lira+18), CTS C30.10, HE 0414, HE 0435: 69 sources

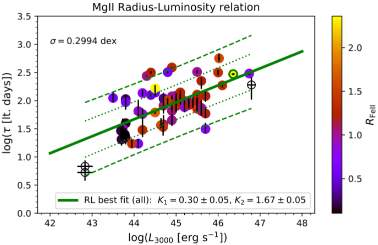

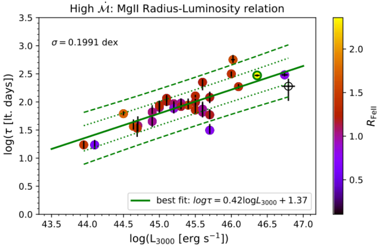

$\log\tau_{\rm obs}$	K_1	K_2	K_3	$\sigma_{\rm rms}$ [dex]	r	$\sigma_{\rm rms}$ [dex] (without)	r (without)
$K_1 \log L_{44} + K_2$	0.422 ± 0.055	1.374 ± 0.082	$\cdots$	0.1991	0.80	0.2012	0.78
$K_1 \log L_{44} + K_2 \log {\rm FWHM}_3 + K_3$	0.43 ± 0.06	-0.13 ± 0.31	1.44 ± 0.17	0.1986	0.80	0.2007	0.78
$K_1 \log L_{44} + K_2 \log R_{\rm Fe\,II} + K_3$	0.45 ± 0.05	0.84 ± 0.29	1.28 ± 0.08	0.1734	0.85	0.1718	0.84
$K_1 \log L_{44} + K_2 \log F_{\rm var} + K_3$	0.39 ± 0.06	-0.38 ± 0.18	0.99 ± 0.19	0.1861	0.83	0.1863	0.82

MgII Radius-luminosity relation

Combining 69 sources with 25 OzDES measurements (Yu+23), we obtain 94 measurements with the redshift range of $0.0041 \leq z \leq 1.89$ (see Prince+2023)

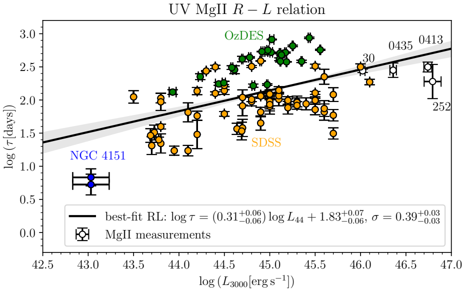

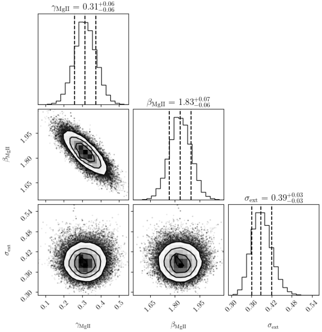

MgII R-L relation and the 2D and 1D likelihood distributions

Comparison of MgII and FeII R-L relations

- first UV FeII R-L relation based on 4 measurements presented in **Prince+(2023)**
- comparison with optical FeII and MgII R-L relations
- NGC 5548: UV FeII time delay by Maoz+1993, MgII by Clavel+1991

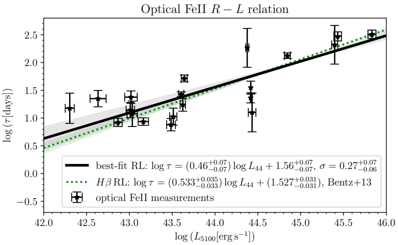

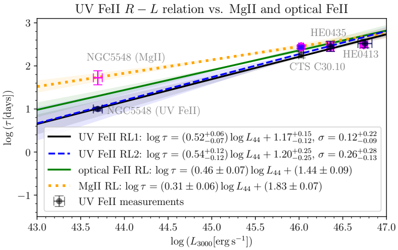

Optical and UV FeII R-L relations vs. MgII R-L relation

Comparison of MgII and FeII R-L relations: distribution

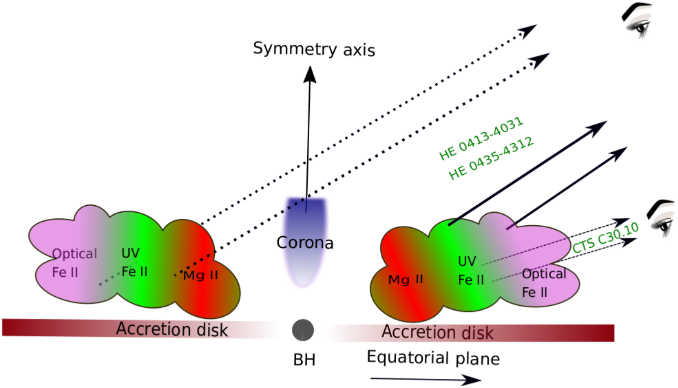

R-L relations + wavelength-resolved RM (Prince+22,23)

CIV Radius-luminosity relation

First constrained HIL radius-luminosity relation, $0.001064 \leq z \leq 3.368$, 38 sources were collected and analyzed by Kaspi et al. (2021).

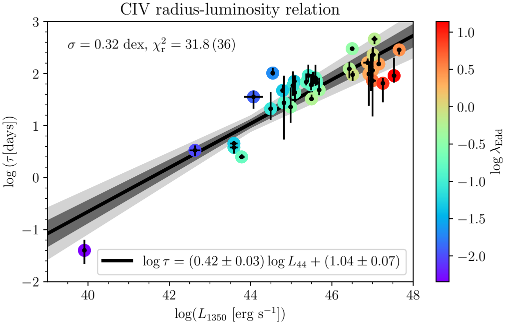

Taken from Cao, Zajaček et al. (2022)

Datasets

RM QSO data

applied for **simultaneously constraining R-L relation as well as cosmological model parameters**. A better established BAO+$H(z)$ combined sample was used as a comparison sample.

Sample	Source number	Redshift range	Reference
Hβ RM QSOs	118	$0.0023 \leq z \leq 0.89$	Khadka+22
MgII RM QSOs	69/78	$0.0033 \leq z \leq 1.89$	Khadka+21
CIV RM QSOs	38	$0.001064 \leq z \leq 3.368$	Cao+22
BAO	12	$0.122 \leq z \leq 2.334$	Cao & Ratra 2022
$H(z)$	32	$0.07 \leq z \leq 1.965$	

Table: Overview of used RM QSO data and the BAO+$H(z)$ comparison sample. BAO+H(z) data are adopted from Tables 1 and 2 in Cao & Ratra 2022, MNRAS, vol. 513, p. 5686-5700.

RM QSOs as standardizable candels

1. Perform reverberation mapping $\rightarrow$ continuum−broad line time lag $\tau_{\rm obs}$
2. Use radius−luminosity (R-L) relation to calculate theoretical time lags $\tau_{\rm th}$

$$\log\left(\frac{\tau_{\rm th}}{\rm day}\right) = \beta + \gamma \log\left[\frac{L_{\rm mon}(z,\mathbf{p})}{10^{44}\,{\rm erg\,s^{-1}}}\right],$$

   $L_{\rm mon} = 4\pi D_{\rm L}(z,\mathbf{p})^2 \lambda F_{\lambda}$, where the luminosity distance is a function of the cosmological expansion rate $H(z,\mathbf{p})$, which depends on the considered cosmological model.
3. Maximize likelihood function to find simultaneously **R-L relation (β, γ) and cosmological model parameters p**

RM QSOs as standardizable candels

3. Maximize likelihood function

$$lnLF = -\frac{1}{2}\sum_{i=1}^{N}\{\frac{[\log\tau_i^{\rm obs} - \log\tau_i^{\rm th}]^2}{s_i^2} + ln(2\pi s_i^2)\}$$

$$s_i^2 = \sigma^2_{\log\tau_{\rm obs,i}} + \gamma^2\sigma^2_{\log F_{3000,i}} + \sigma^2_{\rm int}$$

- 6 cosmological models: flat and non-flat ΛCDM, XCDM, and ϕCDM
  $H(z) = H_0\sqrt{\Omega_{m0}(1+z)^3 + \Omega_{k0}(1+z)^2 + \Omega_{\rm DE}(z)}$,
  For ΛCDM and XCDM: $\Omega_{\rm DE}(z) = \Omega_{\rm DE0}(1+z)^{1+\omega_{\rm X}}$
  ϕCDM (Peebles & Ratra 1988, Ratra & Peebles 1988):
  $V(\phi) = \frac{1}{2}\kappa m_{\rm p}^2\phi^{-\alpha}$ represents scalar field potential energy density
  $\Omega_{\rm DE} = \Omega_\phi(z,\alpha) = \frac{8\pi\rho_\phi}{32 m_{\rm p}^2 H_0^2}$

Constraints from MgII sample

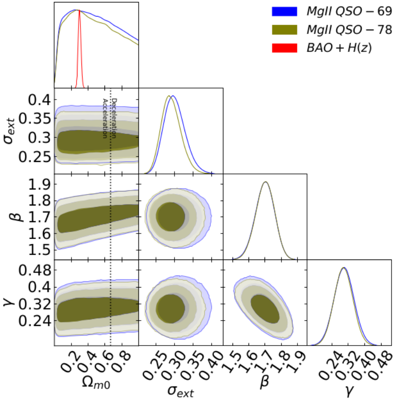

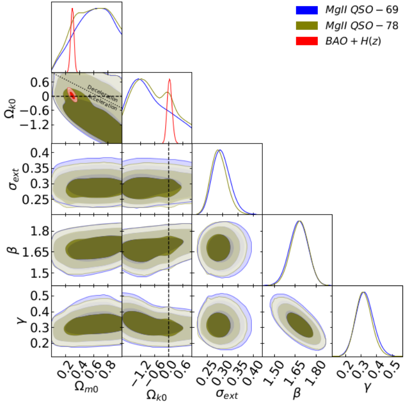

Likelihood distributions and contours for **flat (left)** and **non-flat (right)** ΛCDM model (see Khadka, Yu, Zajaček et al. 2021).

Constraints from MgII+CIV+BAO+H(z) sample

Consistent with BAO+H(z) – exemplary likelihood distributions for non-flat ΛCDM

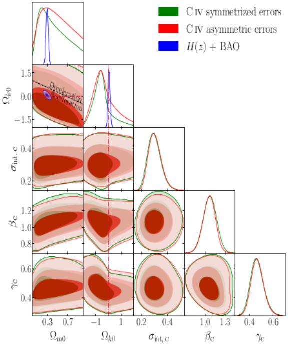

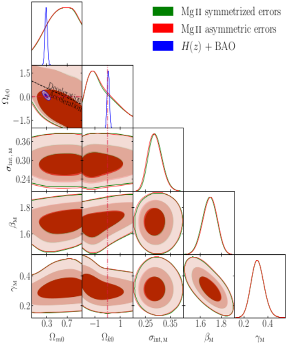

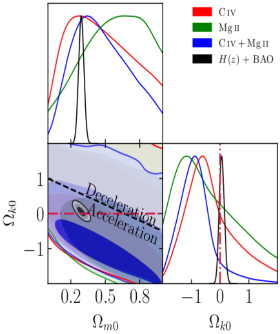

CIV and MgII quasars and their combination (Cao, Zajaček et al. 2022)

Constraints from MgII+CIV+BAO+H(z) sample

Consistent with BAO+H(z) – exemplary likelihood distributions for non-flat ΛCDM

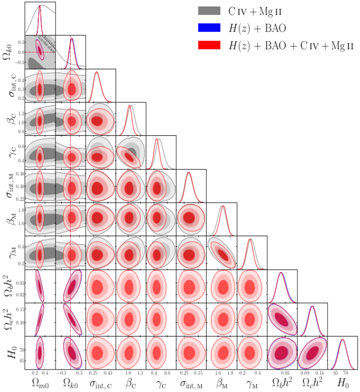

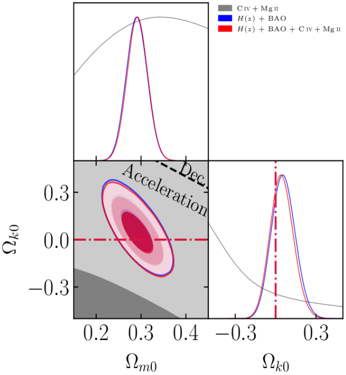

CIV and MgII quasars analyzed jointly with BAO+H(z) (Cao, Zajaček et al. 2022) $\rightarrow$ **quasars slightly tighten the constraints** ($\sim 0.1\sigma$ at most)

Hβ sample

- lower-redshift sample
- constraints in $\sim 2\sigma$ tension with BAO+$H(z)$ (**preference for decelerated expansion**)

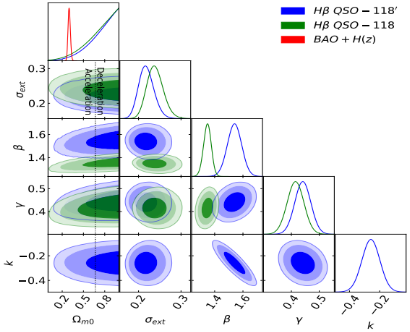

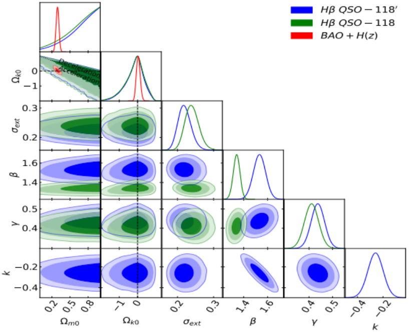

Likelihood contours for **flat (left)** and **non-flat (right)** ΛCDM model (see Khadka, Martinez-Aldama, Zajaček et al. 2022).

Putting it all together

- Hubble diagram combining Hβ, MgII, and CIV RM QSOs with the maximum-likelihood flat ΛCDM model.

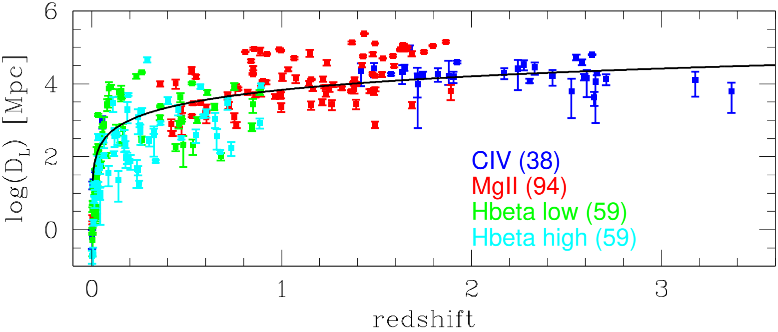

Figure: Hubble diagram of RM quasars (Hβ, MgII, and CIV) with the black solid line showing the inferred flat ΛCDM model with $H_0 = 68.86\,\mathrm{km\,s^{-1}\,Mpc^{-1}}$ and $\Omega_{\rm m0} = 0.295$.

Conclusions

- MgII line is significantly variable and responds to the UV continuum emission,
- **MgII R-L relation shows a significant correlation but is flatter than both Hβ and UV FeII relations**,
- MgII (and CIV) R-L relation is independent of a cosmology model, and thus **can be applied to standardize RM quasars**,
- cosmological constraints from reverberation-mapped quasars are weaker in comparison with BAO+H(z) data,
- for MgII and CIV quasars, constraints are consistent with BAO+H(z) (Khadka et al. 2021, Cao et al. 2022). However, for Hβ quasars, there is $\sim 2\sigma$ tension with BAO+H(z) constraints (Khadka et al. 2022),
- the joint analysis MgII+CIV+BAO+H(z) leads to mildly tighter cosmological constraints (at most $\sim 0.1\sigma$) in comparison with BAO$+H(z)$ sample alone (Cao et al. 2022).

$R - L$ vs. $L_X - L_{UV}$ relation

- a sample of 58 X-ray detected reverberation-mapped quasars
- systematic differences between the two relations
- $L_X - L_{UV}$ shows preference for high Ω_{m0}

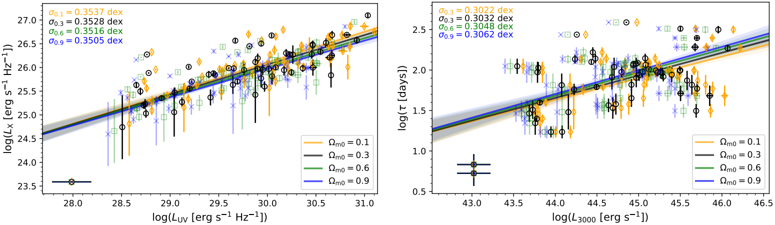

Left: $L_X - L_{UV}$ relation; Right: $R - L$ relation (Khadka, Zajaček et al., MNRAS in print)

$R - L$ vs. $L_X - L_{UV}$ relation

- a sample of 58 X-ray detected reverberation-mapped quasars
- systematic differences between the two relations
- $L_X - L_{UV}$ shows preference for high Ω_{m0}

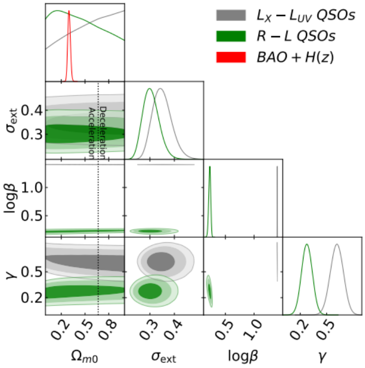

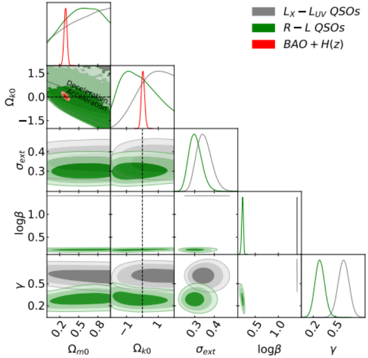

Likelihood distributions for ΛCDM (Khadka, Zajaček et al., MNRAS in print)

$R - L$ vs. $L_X - L_{UV}$ relation

- normally, both relations should give the same luminosity distance to the same source
- however, we obtain non-zero median luminosity distance difference $\log D_{L,L_X-L_{UV}} - \log D_{L,R-L}$, systematically positive

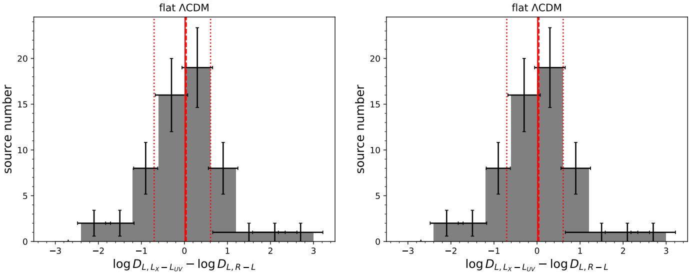

Simple formula for UV/X-ray colour index:

$$E_{X-UV} = 2.172(1-\gamma') < (\log D_{L,L_X-L_{UV}} - \log D_{L,R-L})_{\rm ext} >$$

MASARYK
UNIVERSITY